Real-time Multi-channel System for Beat to Beat QT Interval Variability

Vito Starc, MD, PhD* and Todd T. Schlegel, MD**

* Institute of Physiology, School of Medicine, University of Ljubljana, Ljubljana, Slovenia

** NASA Johnson Space Center, Human Adaptation and Countermeasures Office, Houston, TX, USA

Short title: Real-time Multi-channel QTV

Authors address:

Vito Starc, MD

Ljubljana University School of Medicine

Institute of Physiology

Zaloska 4

1104 Ljubljana

Slovenia

Tel: +386 1 543 7500

Fax: +386 1 543 7501

E-mail: vito.starc@mf.uni-lj.si

Grant No.: PO-510-381

Ministry of Education, Science and Sport

Slovenia

ABSTRACT

The measurement of beat-to-beat QT interval variability (QTV) shows clinical promise for identifying several types of cardiac pathology. However, until now, there has been no device capable of displaying, in real time on a beat-to-beat basis, changes in QTV in all 12 conventional leads in a continuously monitored patient. While several software programs have been designed to analyze QTV, heretofore, such programs have all involved only a few channels (at most) and/or have required laborious user interaction or off-line calculations and post-processing, limiting their clinical utility. This paper describes a PC-based ECG software program that in real time, acquires, analyzes and displays QTV and also PQ interval variability (PQV) in each of the eight independent channels that constitute the 12-lead conventional ECG. The system also processes certain related signals that are derived from singular value decomposition and that help to reduce the overall effects of noise on the real-time QTV and PQV results.

Introduction

The measurement of beat-to-beat QT interval variability (QTV) shows clinical promise for identifying several types of cardiac pathology, including coronary artery disease(1-3), acute myocardial ischemia(4) and infarction(5), left ventricular hypertrophy(6) and various types of cardiomyopathy(7-9). Importantly, in patients referred for electrophysiologic studies and in animals who receive drugs that prolong the QT interval, increased repolarization lability as reflected by increased beat-to-beat QTV is strongly predictive of future arrhythmic events(10, 11). As such, several researchers have recently developed software programs to quantify QTV. There are, however, a number of limitations associated with these existing software programs. First, most if not all require that the operator actively perform certain functions, for example that he or she manually choose the onset and offset of an initial QT interval template. This step of human intervention is both time- and labor consuming, and affects reproducibility(12). Second, the majority of these existing programs also allow for QTV analyses in only one single channel at a time (i.e., usually in limb lead II or limb lead I), and not in multiple channels simultaneously. This can lead to spuriously high QTV values, particularly when the T wave in the channel being studied is small, noisy or otherwise poorly defined. Third, to our knowledge, no existing programs for QTV analyses perform in real time, only offline, with the exception of one real-time program that is focused on dynamic QT vs. RR plots(13) and which in any case has the other limitations noted above. A lack of real-time capability necessarily entails that any acute or subacute *change* in QTV, as might occur for example during myocardial ischemia(4) (or the treatment thereof), cannot be readily observed or acted upon. All of these same limitations also apply to existing software designed to analyze PQ interval variability (PQV)(14-16).

We describe herein a PC-based software program that allows for the real-time monitoring of multiple indices of QTV and PQV, simultaneously in each of the 8

independent channels that constitute the standard 12-lead ECG. The program also contains utilities for automatic formation of templates and detection of intervals such that dependencies on the operator are completely eliminated. In addition, several self-adjusting procedures control the software's associated signal averaging techniques and thus provide quality control for the consistent determination of the QT and other intervals. These iterative averaging techniques ensure more precise determinations of QTV and PQV by preventing the analysis of noise and by eliminating important artifacts such as jitter in the detected QRS-wave fiducial points. As a result, several indices of variability are provided instantaneously and on a beat-to-beat basis, allowing for the online monitoring of multiple cardiac electric processes. The program's analysis of ECG waveforms consists of first identifying individual beats and then particular waves, followed by the formation of template beats, construction of time series for the RR, QT and PQ intervals, and finally the statistical description of the variability of the last "n" recorded beats for each interval type. The performance of the software – especially with respect to the stability and precision of key measured indices – is also briefly illustrated herein through a study that involved 12-lead ECG recordings during both normal breathing and during deep, slow breathing in 19 healthy individuals.

Software methods

The real-time analysis of QTV and PQV is performed on a Windows 2000 or XP-based PC using a "client" software program ("PQT", developed in Slovenia) that communicates with a "server" software program (CardioSoft, Houston, TX). The communication between the client and server software is established via a Windows-based named pipe. A commercial 12-lead PC-based ECG device (e.g., CardioSoft, Houston, TX or Cardiax, IMED, Budapest, Hungary) provides eight channels of incoming raw ECG data via the named pipe to the client at a sampling rate of 1 ms.

Two processes run in parallel within the PQT client: the acquisition of data and ECG wave analysis. Both processes run in a time-shared mode controlled by two separate threads on the Windows 2000 or XP-based PC. The first thread reads the named pipe to which raw data are provided by the server program, which results in the writing of eight channels of ECG data into a circular buffer that can contain up to the last "M" minutes of 1 ms-sampled data. Besides the raw data, the commercial 12-lead PC-based ECG devices also provide the positions of the instantaneous QRS-wave fiducial points. The PQT client program uses this information as well as information from its own QRS-wave detector to perform assessments of the amount of QRS-wave jitter.

Beat selection for averaging

When analysis begins, templates for the overall ECG signal in each channel are first formed. These initial global templates are formed somewhat differently from later templates. To construct the initial global templates, the first 20 beats are collected, the probability function(17) of the RR interval is created for those beats, and its maximum determined. Finally, those ten beats that are closest to the determined maximum are selected, and a template ECG wave for the same beats is then obtained by superimposing the ECG signal based on the fiducial point of the QRS wave. When later ECG templates are constructed, separate templates for the QRS complex and for the T and P waves are formed as described below.

Automated formation of separate templates for the QRS, T and P waves

After the initial templates have been constructed, breaking points called PQ_{break} (between the P wave and the QRS complex), QT_{break} (between the QRS complex and the T wave), T_{end} (the final point of the T wave) and P_{ini} (the initial point of the P wave) are used to

construct templates for the three principal waveforms QRS, T and P. Thus, the QRS complex will ultimately be confined to the time interval between PQ_{break} and QT_{break}, the T wave to the time interval between QT_{break} and T_{end}, and the P wave to the time interval between P_{ini} and PQ_{break}. The algorithms that define the breaking points and thus the templates themselves are described below.

a. QRS template

The characteristics of the template QRS complex are determined by searching for local minima and maxima as well as by the minimal and maximal time derivative values (slopes) between them (Figure 1). The initial slope is defined as the first deflection before the fiducial point that is larger than 1/10 of the maximal slope of the given QRS complex. The crossing of the initial slope with the preceding nearly horizontal segment determines the initial point of the QRS complex, Q_{ini}, for each measured ECG lead. Next, the program selects the first segment of the QRS complex that is larger than 15% of the total QRS signal amplitude, and determines the first and the last point of that segment, QRS_1 and QRS_2, respectively (Figure 1). This segment is used to determine the ΔQRS, the deviation of the initial part of the QRS complex of the incoming beat from the same region in the template. This is necessary to correct any QRS shift (jitter) or an improperly detected fiducial point for the incoming signal.

The time instant of the Q_{ini} points obtained from all eight measured signals are then treated statistically to find the mean and the standard deviation (SD), and a point called Q_{ini0} is defined as the earliest of the eight Q_{ini} that occurred within one SD from the mean. The final point of the QRS complex, QRS_{end}, is determined similarly to Q_{ini}, and then the point QRS_{end0} is determined similarly to Q_{ini0}. It is Q_{ini0} and QRS_{end0} that in turn determine the breaking points (PQ_{break} and QT_{break}) between waves. Specifically, in the present

implementation of the program, PQ_{break} is considered to occur 20 ms before $Q_{ini0,}$ and QT_{break} 30 msec after QRS_{end0}.

When PQ and QT variability are determined, the borders for the QRS template (Q_{ini0} and QRS_{end0}) as well as the QRS breaking points (PQ_{break} and QT_{break}) are treated as the same for all leads. However, new borders and breaking points are computed every time the program (through automatic pre-set) or the user (through manual interaction) instigates a new template in order to optimally refresh the monitoring going forward.

b. T wave template

The onset and offset of the T-wave template are constructed in the following manner. First, a biparabolic curve is constructed consisting of two interconnected parabolic segments, both with an amplitude one half of the total biparabolic curve height, the first part nearer to the QRS complex and the second (distal) part with its apex convex toward the zero line (Figure 2). The first and the last point of the biparabolic curve are designated as T_1 and T_2, respectively. Both parabolic segments are further divided into three parts, with the apex occurring in the outer third of each parabola. The apex of the distal parabola is later used to determine the final point of the T wave, T_{end}. In addition, in order to more closely replicate the T wave, the horizontal line between points T_{end} and T_2 replaces the most distal aspect arising from T_{end}. The biparabolic curve is shifted toward the QRS complex, while varying its height and width until finding the best fit to the initial template T wave. Because for waveforms in both the positive and negative directions, several matches might have occurred while approaching from the distal part towards the QRS complex, the one with the largest overall amplitude is selected as the most representative one. The point T_{end} is then determined by the position of the distal apex point. The interval $QT_0 = T_{end} - Q_{ini0}$ is then the absolute duration of the QT interval in that particular ECG lead. In addition to determining T_{end}, the

program uses both of the extremities of the representative biparabolic curve, T_1 and T_2, to determine the interval for matching the incoming T_{end} to the T_{end} of the existing template. However, unlike the case for the QRS template borders and breaking points, T_{end} is subsequently treated as unique for each lead.

c. P wave template

A procedure similar to that used to form the T-wave template is also used to determine the appropriate borders for the P wave template in all ECG leads. In addition, once determined, P_{ini}, like T_{end}, is subsequently treated as unique for each lead.

QT interval variability algorithm

In the PQT program, the P, QRS and T templates are constructed by signal averaging rather than by using a single beat from the measured ECG signal. In addition, matching of any new incoming complex to the templates in any region of interest is thereafter achieved by *shifting* of the ECG signal(1, 2, 16), not by "stretching"(8). It should be understood that the PQT program is principally concerned with quantifying the variability of intervals rather than their absolute values. Thus, if for any reason the algorithm chooses a false beginning or end point for a given template interval, then all interval values will be biased proportionately, but the beat-to-beat variability in the computed intervals will be unaffected. The specific steps performed in analyzing QT interval variability are described in detail below.

1) The template beat $\varphi(n)$, where n is the sample number, is constructed from the selected beats using a signal averaging technique. Only those beats with shape similar to the template are selected for averaging. Since the program automatically determines the borders of each wave component (P, QRS, and T templates, as described above) and therefore the time window for matching of waves, its remaining task is to shift the particular incoming

wave component with respect to the template until obtaining an acceptable match. The matching algorithm is based on the least square deviation of the incoming wave versus the template.

2) The matching of waves is performed in two sub-steps. First, a broader time interval containing the complete wave component is used to reach the best fit. Specifically, the points QT_{break} and T_2 are used for the T wave (Figure 3a), PQ_{break} and QT_{break} for the QRS complex, and P_1 and PQ_{break} for the P wave. In this sub-step, the amplitude of the incoming wave component is normalized with respect to the template, i.e., it is adjusted to reach the same surface area under the curve in the same time interval as that of the template (Figure 3a). This sub-step is important for providing a parameter called the "norm", an index of the quality of matching described in greater detail below. In the second sub-step, shifting of the normalized wave in time is performed to achieve the best fit in a smaller time window. Specifically, the points T_1 and T_2 define the best fit for the end of the T wave (Figure 3b), the points QRS_1 and QRS_2 the best fit for the beginning the QRS complex, and the points P_1 and P_2 the best fit for the beginning of the P wave.

3) Each wave of any incoming beat x(n) is shifted to or from the trigger point to achieve the best alignment with the template in the appropriate time window. For this purpose, an error function of time shifting $\varepsilon_i(a_k)$ is defined as the sum of the squared differences between the template wave (P, QRS or T) and the appropriate shifted version of the incoming wave of beat *i*:

$$\varepsilon_i(a_k) = \sum_{j=n_1}^{n_2} \left[\varphi(T_k + j) - x(T_i + a_k + j)\right]^2$$

where a_k is the time-shifting parameter of ECG lead *k*, T_k is the triggering point of the template, T_i is the triggering point of the beat *i*, and n_1 and n_2 are the beginning and the end of the matching windows, e.g., QT_{break} and T_2 in the first matching, and T_1 and T_2 in the second matching, respectively, in the case of the T interval. The parameter a_k is changed for that beat

to find that particular a_k, called $\hat{a}_k$, which occurs at the minimal $\varepsilon_i(a_k)$ until the step of a_k is < 0.1 ms. To achieve shifting of the P, QRS and T waves by a noninteger value of a, interpolation of the waves between the measured sampled values is necessary.

4) The value of $\varepsilon_i(a_k)$ after the first matching represents the quality of matching, or the norm. The norm is mathematically a dimensionless quantity that represents the average deviation of the incoming wave from the template, divided by the amplitude (A) of the wave in that interval; i.e., norm = $\sqrt{\varepsilon_i(a_k)}/(n_2 - n_1+1)/A$. The lower the norm, the better the fit, and when the incoming wave and the template are perfectly matched, the norm = 0.

During construction of the template, the norm in each particular ECG lead is treated statistically to obtain the mean value and SD in that lead. The match between the incoming wave and the template is considered acceptable if the norm of any beat is within one SD of the mean norm in the corresponding ECG lead. This procedure helps in providing an acceptable number of beats for averaging even in case of noisy signals. For the QRS and T waves, an acceptable norm is usually less than 0.15.

5) Instead of using a single bin for the signal averaging of any particular ECG waveform, the PQT program uses seven bins that cover the expected variability interval of each waveform type. Hence, for QT variability, the first bin is used for averaging of the shortest QT intervals, and the successive bins for averaging of successively longer QT intervals. The variability interval is defined from the variability record during previous construction of the template, and is initially set to 15 ms. Thus, for example, if the T wave variability interval in lead II was 14 ms during template construction, then each bin for averaging will be 2 ms wide. Before adding the wave into the corresponding bin for signal averaging, the wave is appropriately shifted to adjust for jitter in that particular bin. This creation of several bins for signal averaging helps to prevent an over-reliance on initial values. At least seven templates are therefore constructed for each waveform in each ECG

lead, and the bin with the highest number of accepted beats is the one ultimately selected to provide the template. The norm is therefore not the only criterion controlling the averaging procedure, and the final percentage of beats that ultimately constitute a template is typically between 35 and 50%. Despite the potential for a reduction in the number of beats, the quality of the template is nevertheless improved due to selection of the most similar beats.

6) It is expected that QT intervals differ among different leads. Hence, the $QT_{k,i}$ interval of *i*-th incoming beat and of *k*-th ECG lead differs from the template $QT_{k,0}$ by an amount $QT_{k,i}$:

$$QT_{k,i} = QT_{k,0} + \Delta QRS_i + \Delta T_{k,i}$$

where $\Delta T_{k,i}$ is the interval obtained by shifting the $T_1 - T_2$ segment of the *i*-th T wave to match the template, and ΔQRS_i by shifting the $QRS_1 - QRS_2$ segment of the QRS complex, respectively.

In detail, the sum of time displacement of the T ($\Delta T_{k,i}$) and QRS waves (ΔQRS_i) forms the QT interval change for the *i*-th beat and the *k*-th ECG lead ($\Delta QT_{k,i}$), and is calculated according to the equation:

$$\Delta QT_{k,i} = \Delta T_{k,i} + \Delta QRS_i$$

where

$$\Delta T_{k,i} = \hat{a}_{k,i(T)}\Delta t, \text{ and } \Delta QRS_i = \hat{a}_{i(QRS)}\Delta t$$

and where $\hat{a}_{k,i(T)}$ and $\hat{a}_{i(QRS)}$ represent the time-shifting factors of the T and QRS wave matching windows and Δt the digitalization interval (1 ms). Because Q_{ini0} (and QRS_{end0}) is the same for all leads, this same procedure also applies to ΔQRS_i. The latter is selected among all eight measured ECG channels as that $\Delta QRS_{k,i}$ which is placed to the time instant of the highest density of the $\Delta QRS_{k,i}$ distribution, using a technique(17) similar to that described for selection of the initial 20 beats with respect to the RR interval. We have found that such

ΔQRS_i differ less than 0.3 ms from a corresponding ΔQRS change obtained from the derived vector ECG using the method of Edenbrandt and Pahlm(18).

Finally, the QT interval for the *i*-th beat is calculated according to the equation:

$$QT_{k,i} = QT_{k,0} + \Delta QT_{k,i}$$

where $QT_{k,0}$ is the duration of the template QT interval in the *k*-th lead.

The algorithm thus provides the QT interval for each beat such that the T wave and QRS complex best match the template T wave and QRS complex under the time-shift model.

PQ interval variability algorithm

The sum of time displacement of the P ($\Delta P_{k,i}$) and QRS waves (ΔQRS_i) constitutes the PQ interval change for the *i*-th beat and of *k*-th ECG lead ($\Delta PQ_{k,i}$) and is calculated according to the equation:

$$\Delta PQ_{k,i} = \Delta P_{k,i} + \Delta QRS_i$$

where

$$\Delta P_{k,i} = \hat{a}_{k,i\,(P)}\Delta t, \text{ and } \Delta QRS_i = \hat{a}_{i(QRS)}\Delta t$$

and where $\hat{a}_{k,i(P)}$ and $\hat{a}_{i(QRS)}$ represent time-shifting factors of the P and QRS wave matching windows and Δt the digitalization interval (1 ms).

Finally, the PQ interval for the *i*-th beat is calculated according to the equation:

$$PQ_{k,i} = PQ_{k,0} + \Delta PQ_{k,i}$$

where $PQ_{k,0}$ is the duration of the template PQ interval.

Time series analysis

The PQT program uses the QTV algorithm as described above to generate, in real time, the time series of the QT interval along with that of the RR interval. Time series are analyzed according to the recommendations of the Task Force of the European Society of Cardiology and the North American Society of Pacing and Clinical Electrophysiology(19)

using specific indices such as the standard deviation of normal-to-normal RR and QT intervals (SDNN RR and SDNN QT, respectively), the root mean square of the successive interval difference (rMSSD RR and RMSSD QT), etc. In addition, real-time changes in related indices that attempt to "correct" QTV (or PQV) for simultaneous variability in RR intervals (see for example (1, 2, 16)) can also be enabled if appropriate, as can (principally for academic reasons(20)) a beat-to-beat QT dispersion function (21) for real-time display.

The Multilead QT interval signal

Because the standard ECG provides several leads in which the QT signal varies in a similar manner with time, the PQT program constructs a "multilead" QT signal, defined as an average of the four most similar signals from the eight independently measured ECG channels. The multilead QT interval is specifically derived in the following way: In each of the eight measured signals, an average QT interval value for the last n beats is calculated, QT_{av}, which is in turn subtracted from each of the individual QT intervals within the n beats to obtain the deviation from the mean, $QT\text{-}QT_{av}$. In case of the *k*-th lead, the result is denoted as $dQT_{k,i} = QT_{k,i} - QT_{av,k}$. For each of any two mutually considered signals, *k*-th and *l*-th, a covariance of the median beat for the n-beats interval is computed as:

$$Cov(QT_k, QT_l) = \sum_{i=1}^{n} (dQT_{k,i} - dQT_{l,i})^2 /(n-1).$$

We thus obtain 8*7/2 = 28 separate covariance values from the eight ECG channels.

Subsequently, the program accepts those half of the channels that overall have the most similar variations and rejects those half that have the least similar variations. Suppose for example that a particular ECG channel appeared in *j* mutual covariances in the accepted set. The program sums all of those covariances, divides the sum by the number *j*, and then takes the square root of the result to get a complex covariance value. Finally, both for this channel and for the other seven independent ECG channels, it calculates the time average

over the last n-beat covariance values and sorts the ECG channels by those values to select the four channels with the most similar QT signals. The time averaging is necessary to retain some stability in case of occasional signal artifact in the accepted ECG channels. The four accepted ECG channels are then used for the construction of the multilead QT interval signal simply by taking the average of their corresponding QT interval values for each ECG beat. The time series of the QT interval thus obtained represents an idealized time series derived from the four channels containing the most similar information, thereby reducing the effects of noise. In addition, for each beat the program calculates the SD of the four accepted QT signals from their mean, a quantity called "QT_{dev}". The QT_{dev} is not only a measure of the quality of the derived multilead QT interval signal, but also of the *spatial* variability in the selected ECG channels. When the beat-to-beat spatial variability (QT_{dev}) is less than the simultaneous beat-to-beat *temporal* variability for the multilead QT interval (also measured as SD), then the temporal variability is more likely a consequence of genuine (as opposed to noise-related) fluctuations.

Selecting only four ECG channels for determination of the multilead QT interval signal tends to eliminate those ECG channels that produce spurious QTV values due to poor delineation of the T and/or QRS waveforms. In relatively noise-free recordings wherein the waveform peaks and troughs are well defined, a high QT_{dev} might theoretically be a consequence of true regional differences (heterogeneity) in repolarization, but this hypothesis has not yet been investigated.

QTRR cross correlation

A cross correlation is also determined between the multilead QT interval and the RR interval for the last n beats. This is calculated as a covariance between the RR and QT interval signals, cov(QT, RR), divided by the square root of each variance:

$QTRR_{xc} = cov(QT, RR)/\sqrt{} QT_v \sqrt{}RR_v$.

It is expected that $QTRR_{xc}$ will approach 1.0 if QT and RR intervals vary in parallel, and –1.0 if they vary in the opposite way, with low absolute $QTRR_{xc}$ values occurring if variations of QT and RR signals are poorly correlated, as is common in disease(8, 22). Although the program calculates $QTRR_{xc}$ between the RR interval and the QT in each of the eight measured ECG channels, the $QTRR_{xc}$ obtained from the multilead QT interval signal provides a singularly representative measure for practical use.

QT and PQ variability based on decomposed signals

The PQT program also calculates ECG waves along the principal axes, obtained by singular value decomposition (SVD)(20, 23, 24) of the incoming eight channels of raw data. In this technique, the ECG is reconstructed after SVD in an orthogonal eight lead system, the first 3 orthogonal components of the T wave representing the traditional 3-dimensional T wave vector or dipolar signal contents. The abundancy of each component is given by its maximal value along its principal axis (eigenvalue). However, because the overall electrode placement in standard ECG is predominantly oriented along the ventricular axis, the eigenvalue of the main orthogonal component obtained by SVD is usually several times larger than that of any individual standard lead. The program therefore employs a modified SVD algorithm to construct the complete ECG signal, including the T wave and QRS complex along the principal axes. Specifically, it attenuates each of the measured ECG signals by that amount required to reach the isotropic distribution with respect to the signal's orientation in space. As an approximation, the program employs a method similar to that of Edenbrandt and Pahlm(18), who reconstructed the Frank vector ECG (x, y and z leads) from the standard leads. However, it uses the multiplication factors a_x, a_y, and a_z of the x, y and z component of the corresponding lead to calculate the main diagonal, d_k, instead. For the *k*-th

lead, $d_k = \sqrt{(a_x^2 + a_y^2 + a_z^2)}$. Next, the ECG signal of the *k*-th lead is multiplied by d_k and applied in the SVD algorithm. As a result, the principal axes of such an approach nearly coincide with those obtained by the SVD algorithm using the three derived orthogonal leads(18). Since the eigenvalues of the orthogonal ECG components fall rapidly from the first through the eighth orthogonal components, the SVD method represents the least square solution to an over-determined set of linear equations provided by the set of eight measured ECG signals. It is therefore a sound approach to eliminate any kind of superimposed noise.

Because for each of the ECG wave components (P, QRS and T), the third through eighth eigenvalues are usually only a small fraction of the first two eigenvalues, the program uses only the first (or alternatively the first and second) orthogonal signals along the principal axes (SVD_1 and SVD_2) to measure what we have termed the QT_{SVD} and PQ_{SVD} intervals. In addition, the program constructs a diagonal value from the three largest orthogonal components (in the Frank lead system this would correspond to the radius vector amplitude, or RVA) with time course represented by $R_0(t) = \sqrt{(SVD_1(t)^2 + SVD_2(t)^2 + SVD_3(t)^2)}$. The RVA signal can only be positive. Nevertheless, it is the only signal we derive that contains the complete three-dimensional information regarding the beginning and the end of the various intervals. Since the resulting signals show by far the lowest variability in waveform shape when compared to their initial templates (see below), they are used to determine the (so-called) QT_{SVD} and PQ_{SVD} variability. The program also determines the values of the so-called T-wave residuum (TWR)(20, 25, 26) both instantaneously for each beat, and in a sliding-window fashion for the last n signal-averaged beats, independently of the TWR of the template signal.

llustration of software performance: a study of healthy individuals

In order to illustrate the performance of the software, standard supine 12-lead ECGs were recorded for 5 min in each of 19 healthy young male subjects (age range 20-23 years) during both normal breathing and during deep, slow breathing. The deep, slow (~0.1 Hz) breathing was performed to help maximize the RR interval excursions(27) (and thus also the QT interval excursions) so that the stability of software's determinations of the QT_c interval could be assessed. In the same study, we were also interested in determining any regional variation in the quality of the signals as evaluated from the corresponding norm values – i.e., for the P, QRS and T waves in the eight standard channels and in two other derived signals: the first orthogonal SVD signal (SVD_1) and radius vector amplitude (RVA) signal (defined above). Another goal was to compare the spatial variation of the 4 components of the multilead QT interval signal with that same signal's temporal variation. Finally, we also desired to study the relative QRS wave jitter in each signal in order to determine the most appropriate signal selection for Q_{ini}, specifically by measuring the SDNN of the QRS interval within each channel or derived signal. The Institutional Review Board at the University of Ljubljana approved the study, and all subjects, who were awake and in sinus rhythm without any sign of heart disease or conduction disturbance, gave informed consent.

Results

As shown in Table 1, the multilead QT interval and the QT intervals of the SVD_1 and RVA signals exhibited no statistically significant changes during normal breathing compared to deep, slow breathing, although there was a trend toward shortening of the QT intervals during the deep, slow breathing. Since this shortening was paralleled by shortening of the RR interval (from 909.7 ± 147 ms to 834.5 ± 139 ms), we corrected the multilead QT interval according to the formula $QT_c = QT/RR^{0.314}$ (28). The resulting QT_c interval changed from 457.3 ± 18.9 ms to 461.8 ± 21.9 ms, with a relative change of 1.9 ± 1.4%. In other words,

even ignoring any inaccuracy associated with one of the better-validated generic QT_c correction formulas (28), the software determined QT_c across the two different conditions with a precision below 5 ms, or 2% .

As shown in Figure 4 (left side), for all three waveform types (P, QRS and T), the lowest norm values (best performance) during normal breathing generally occurred in the two derived signals rather than in any of the standard leads. Whereas the norm values in standard lead II were amongst the lowest for the P and QRS waves, they were amongst the highest for the T wave, suggesting that lead II is probably *not* the most ideal lead for QTV analyses. In general, the P wave norm values were approximately double those for the QRS and T waves across the various leads. Deep, slow breathing adversely affected the norms in the majority of leads (Figure 4, right side). Nonetheless, one or the other of the derived signals still remained the best overall performer for all three waveform types, regardless of the breathing pattern.

The spatial variability (QT_{dev}) associated with the four constituents of the multilead QT signal was 1.79 ± 0.98 ms during normal breathing versus 2.42 ± 1.3 ms during deep, slow breathing, while the simultaneous temporal variability of the signal as measured by SDNN was 3.14 ± 2.0 ms versus 5.47 ± 4.60 ms, respectively. Thus, given the ratios of spatial to temporal variability, much of the temporal variability was likely genuine and not due to noise.

Values for PQ variability, QRS jitter, and QT variability during normal breathing (all as measured by SDNN) are shown in Figure 5 (left side). During deep, slow breathing, both variability and jitter increased (right side of Figure 5). As with the norm, the mean variability and jitter values were also generally lowest for one or the other of the derived signals.
The QRS jitter value (by SDNN) in lead II during normal breathing was 1.07 ± 0.71 ms. This compares to an actual PQ and QT variability (also by SDNN) of 4.31 ± 1.88 ms and 3.30 ±

1.55 ms, respectively, in the same lead during normal breathing. Thus, QRS jitter itself could theoretically account for up to a quarter of the PQV and up to a third of the QTV in lead II-based calculations. The potential contribution of QRS jitter to PQV and QTV appeared to be even higher during deep, slow breathing.

Finally, Figure 6 shows an example of RR interval variability (panel a) and the corresponding QTV (panel b) in a healthy young male performing deep, slow (0.1 Hz) breathing. As expected, the QT interval mostly followed the RR interval, which resulted in a high absolute value for $QTRR_{xc}$. The quality of matching (norm) in this case was also better for the T wave than for the QRS wave (panel c), while the QRS signal showed considerable jitter with respect to the trigger (panels c and d). As illustrated by this case, the results of QTV using our method (shifting) do not differ in any significant way from those using the method of Berger et al (stretching) when the latter method is also corrected for QRS trigger-point jitter. When such is the case, both methods result in nearly identical QT interval signals and norms for the T wave (panels b and c). Very pronounced though was the exaggerative effect that QRS jitter had on QTV. Thus, in any case where the Berger et al. (or our) method relies strictly on a QRS fiducial point uncorrected for jitter, it results in a distorted (exaggerated) QTV, as shown in panel b.

Summary

In conclusion, our institutions have collaboratively developed an advanced ECG software program that in conjunction with commercially available PC-based ECG hardware and software, acquires, analyzes and displays the QT and PQ variability within each of the independent ECG channels in real time on a beat-to-beat basis. It also performs the same functions utilizing certain derived signals that reduce the effects of both noise and physiological jitter and thus improve the reliability of the overall results. Although additional

clinical validation is necessary, the automated, multichannel, real-time and noise-reduction aspects of the software will hopefully aid in bringing what has heretofore been regarded as a highly promising research technique into eventual clinical usage.

References

1. Vrtovec B, Starc V, Starc R. Beat-to-beat QT interval variability in coronary patients. *J Electrocardiol*. 2000;33(2):119-25.
2. Vrtovec B, Sinkovec M, Starc V, Radovancevic B, Schlegel TT. Coronary artery disease alters ventricular repolarization dynamics in type 2 diabetes. *Pacing Clin Electrophysiol*. 2005;28 Suppl 1:S178-81.
3. Johansson M, Gao SA, Friberg P, et al. Elevated temporal QT variability index in patients with chronic renal failure. *Clin Sci (Lond)*. 2004;107(6):583-8.
4. Murabayashi T, Fetics B, Kass D, Nevo E, Gramatikov B, Berger RD. Beat-to-beat QT interval variability associated with acute myocardial ischemia. *J Electrocardiol*. 2002;35(1):19-25.
5. Nahshoni E, Strasberg B, Adler E, Imbar S, Sulkes J, Weizman A. Complexity of the dynamic QT variability and RR variability in patients with acute anterior wall myocardial infarction: a novel technique using a non-linear method. *J Electrocardiol*. 2004;37(3):173-9.
6. Piccirillo G, Germano G, Quaglione R, et al. QT-interval variability and autonomic control in hypertensive subjects with left ventricular hypertrophy. *Clin Sci (Lond)*. 2002;102(3):363-71.
7. Atiga WL, Fananapazir L, McAreavey D, Calkins H, Berger RD. Temporal repolarization lability in hypertrophic cardiomyopathy caused by beta-myosin heavy-chain gene mutations. *Circulation*. 2000;101(11):1237-42.
8. Berger RD, Kasper EK, Baughman KL, Marban E, Calkins H, Tomaselli GF. Beat-to-beat QT interval variability: novel evidence for repolarization lability in ischemic and nonischemic dilated cardiomyopathy. *Circulation*. 1997;96(5):1557-65.
9. Berger RD. QT variability. *J Electrocardiol*. 2003;36 Suppl:83-7.
10. Atiga WL, Calkins H, Lawrence JH, Tomaselli GF, Smith JM, Berger RD. Beat-to-beat repolarization lability identifies patients at risk for sudden cardiac death. *J Cardiovasc Electrophysiol*. 1998;9(9):899-908.
11. Thomsen MB, Verduyn SC, Stengl M, et al. Increased short-term variability of repolarization predicts d-sotalol-induced torsades de pointes in dogs. *Circulation*. 2004;110(16):2453-9.
12. Gao SA, Johansson M, Hammaren A, Nordberg M, Friberg P. Reproducibility of methods for assessing baroreflex sensitivity and temporal QT variability in end-stage renal disease and healthy subjects. *Clin Auton Res*. 2005;15(1):21-8.
13. Govreen-Segal D, Radai MM, Sivan Y, Abboud S. Real-time PC-based system for dynamic beat-to-beat QT-RR analysis. *Comput Biomed Res*. 1999;32(4):336-54.
14. Forester J, Bo H, Sleigh JW, Henderson JD. Variability of R-R, P wave-to-R wave, and R wave-to-T wave intervals. *Am J Physiol*. 1997;273(6 Pt 2):H2857-60.
15. Shouldice R, Heneghan C, Nolan P, Nolan PG, McNicholas W. Modulating effect of respiration on atrioventricular conduction time assessed using PR interval variation. *Med Biol Eng Comput*. 2002;40(6):609-17.
16. Arnol M, Starc V, Starc R. Atrioventricular conduction variability in coronary patients. *J Electrocardiol*. 2003;36(4):311-9.
17. Press WH. Numerical recipes in C : the art of scientific computing. 2nd ed. Cambridge ; New York: Cambridge University Press; 1992:610-615.
18. Edenbrandt L, Pahlm O. Vectorcardiogram synthesized from a 12-lead ECG: superiority of the inverse Dower matrix. *J Electrocardiol*. 1988;21(4):361-7.

19. Heart rate variability. Standards of measurement, physiological interpretation, and clinical use. Task Force of the European Society of Cardiology and the North American Society of Pacing and Electrophysiology. *Eur Heart J*. 1996;17(3):354-81.
20. Malik M, Acar B, Gang Y, Yap YG, Hnatkova K, Camm AJ. QT dispersion does not represent electrocardiographic interlead heterogeneity of ventricular repolarization. *J Cardiovasc Electrophysiol*. 2000;11(8):835-43.
21. Figueredo EJ, Ohnishi Y, Yoshida A, Yokoyama M. Usefulness of beat-to-beat QT dispersion fluctuation for identifying patients with coronary heart disease at risk for ventricular arrhythmias. *Am J Cardiol*. 2001;88(11):1235-9.
22. Frljak S, Avbelj V, Trobec R, Meglic B, Ujiie T, Gersak B. Beat-to-beat QT interval variability before and after cardiac surgery. *Comput Biol Med*. 2003;33(3):267-76.
23. Press WH. Numerical recipes in C : the art of scientific computing. 2nd ed. Cambridge ; New York: Cambridge University Press; 1992:59-70.
24. Acar B, Yi G, Hnatkova K, Malik M. Spatial, temporal and wavefront direction characteristics of 12-lead T-wave morphology. *Med Biol Eng Comput*. 1999;37(5):574-84.
25. Zabel M, Malik M, Hnatkova K, et al. Analysis of T-wave morphology from the 12-lead electrocardiogram for prediction of long-term prognosis in male US veterans. *Circulation*. 2002;105(9):1066-70.
26. Okin PM, Malik M, Hnatkova K, et al. Repolarization abnormality for prediction of all-cause and cardiovascular mortality in American Indians: the Strong Heart Study. *J Cardiovasc Electrophysiol*. 2005;16:1-7.
27. Bernardi L, Sleight P, Bandinelli G, et al. Effect of rosary prayer and yoga mantras on autonomic cardiovascular rhythms: comparative study. *Bmj*. 2001;323(7327):1446-9.
28. Malik M. Problems of heart rate correction in assessment of drug-induced QT interval prolongation. *J Cardiovasc Electrophysiol*. 2001;12(4):411-20.

Table 1. Changes in intervals after breathing change

QT_{ML}	QT_{SVD1}	QT_{RVA}	RR interval	QT_{cML}
Normal Breathing 442.8±31.1	442.8 ± 30.51	442.3 ± 30.6	909.6 ± 147.6	457.27 ± 18.9
Deep, Slow Breathing 434.7±26.5	437.7 ± 30.7	435.3 ± 25.2	834.5 ± 139.4	461.78 ± 21.9

Values are means ± standard deviations in ms. N = 19 subjects. QT_{ML}, QT_{SVD1} and QT_{RVA}: QT interval values based on the multilead QT interval, SVD1 and RVA signals, respectively. QT_{cML}: the corrected multilead QT interval value. No statistically significant changes in QT intervals were noted by t-test.

Figure Legends

Figure 1. The borders of the template QRS complex are determined by searching for local minima and maxima as well as by the minimal and maximal slopes. The crossing of the initial slope with the preceding nearly horizontal segment determines the initial point of the QRS complex, Q_{ini}, of each measured ECG lead, and the last crossing the point QRS_{end}, necessary for determination of the breaking points between waves, PQ_{break} and QT_{break}, which occur 20 ms before Q_{ini0} and 30 msec after QRS_{end0}, respectively. The points QRS_1, and QRS_2 determine the smaller time window for the final matching of the QRS wave.

Figure 2. To determine the T-wave onset and offset, a biparabolic curve is constructed using two interconnected parabolic segments, both with an amplitude one half of the total biparabolic curve height. The segments are connected at the median point of the biparabolic curve. In the distal parabolic segment a horizontal line replaces the most distal 'hook' between T_{end} and T_2. The initial biparabolic curve (thick solid dark gray curve) is shifted toward the QRS complex, while varying its height and width until finding the best fit to the template T (thick solid black curve). The position of the biparabolic curve then determines the border points on the template wave (dashed curve), for defining the smaller time window for later matching (see Figure 3b). These border points are T_1 and T_2 for the time-shift parameter, and T_{end} for determining the end point of the T wave.

Figure 3. *a*) Initial shifting and normalizing: The incoming wave (taller dashed curve, black) is shifted toward the template wave (solid dark gray curve) for matching. Simultaneously, it is normalized to have the same amplitude in the broader time window from QT_{break} to T_2 (lower dashed curve, black). The squared difference between the

normalized wave and the template represents the norm for the T wave. *b*) Final shifting: The distal segment (lower right dashed curve, black) of the normalized incoming wave (dashed dark gray curve under the template T wave) is shifted further toward the template wave (solid dark gray curve) for matching in the smaller time window from T_1 to T_2. The required total shift from the incoming wave to the final position of the distal segments represents the time shift $\Delta T_{k,i}$.

Figure 4. Norm values for the P, QRS and T waves during normal breathing (left plots) and during deep, slow breathing (right plots) in a group of 19 healthy males. Norm values for the P wave were higher than those for the QRS and T waves, and for all wave types, the performance of one or the other of the derived signals (i.e., of SVD1, the first orthogonal component from singular value decomposition, or of RVA, the radius vector amplitude) was generally superior to that of the best of the eight individual standard channels.

Figure 5. Variability of the PQ, QRS and QT intervals during normal breathing (left plots) and during deep, slow breathing (right plots) in the same group of 19 healthy males. The SDNN (standard deviation of normal intervals) of all three interval types generally increased during deep, slow breathing compared to normal breathing, with the increased variability of the QRS interval reflecting increased "jitter". As with the norm values, the mean variability and jitter values were also generally lowest for one or the other of the derived signals.

Figure 6. QT and other interval variability during deep, slow (0.1 Hz) breathing in a healthy male. Panel a (uppermost) shows the RR interval changes during a 100 s interval. Panel b shows the corresponding changes of the QT intervals in lead V_3. Within panel b, the lower, QRS jitter-corrected QT trends were obtained by the "shifting" method (described herein)

and by the “stretching” method of Berger et al(8), respectively. The two trends are effectively superimposed, demonstrating the practical equivalence of the two techniques. The upper trend in the panel b represents variability of the T wave only, without considering QRS wave variability (“jitter”). Panel c demonstrates that the norms for the T wave also do not differ between the “shifting” and “stretching” methods, although in this case the T-wave norm was considerably lower than that for the QRS. Panel d demonstrates that QRS jitter can be significant, particularly during deep breathing.

Figure 1.

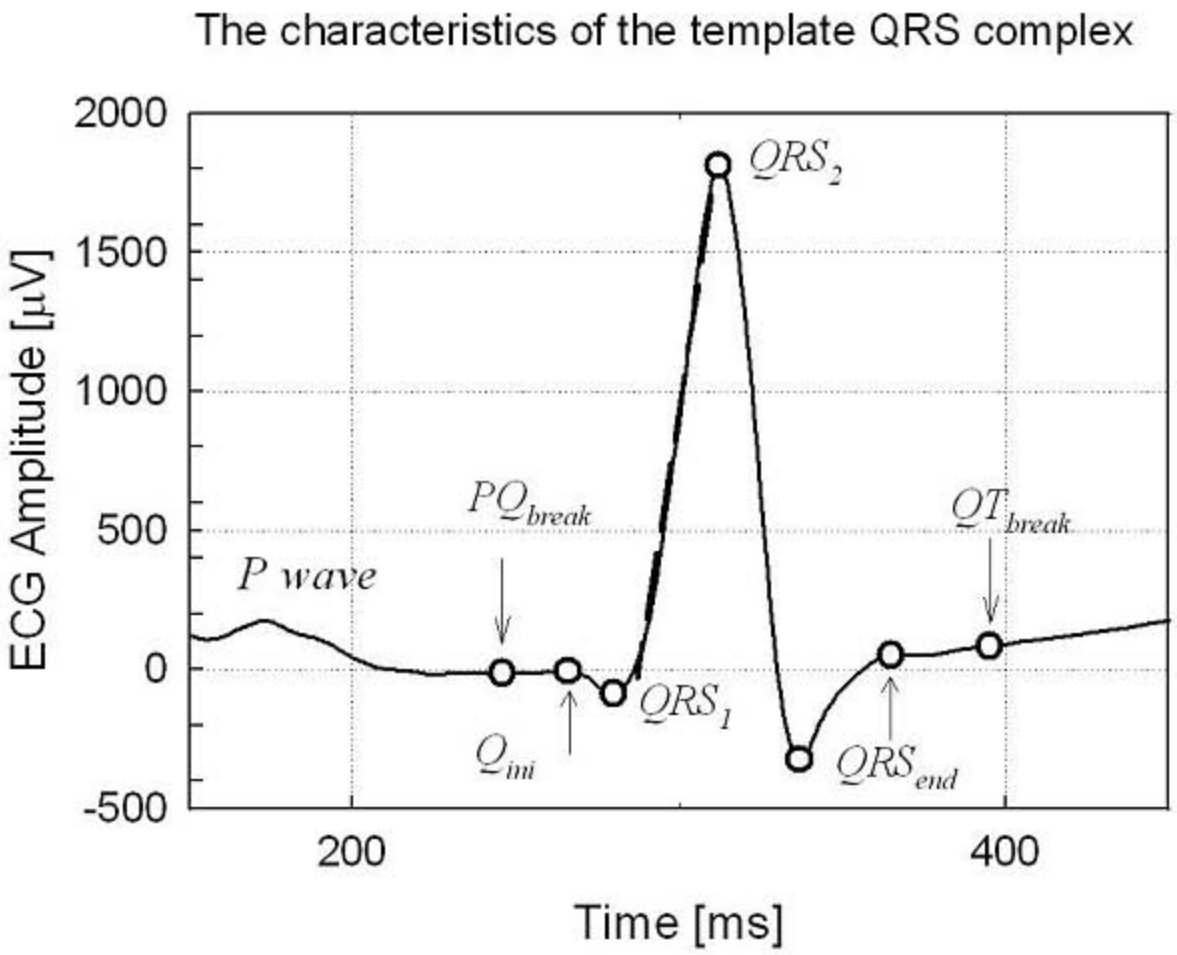
The characteristics of the template QRS complex
ECG Amplitude [μV]
2000
1500
1000
500
0
-500
200
400
Time [ms]
P wave
PQ_{break}
QT_{break}
QRS_2
QRS_1
Q_{ini}
QRS_{end}

Figure 2.

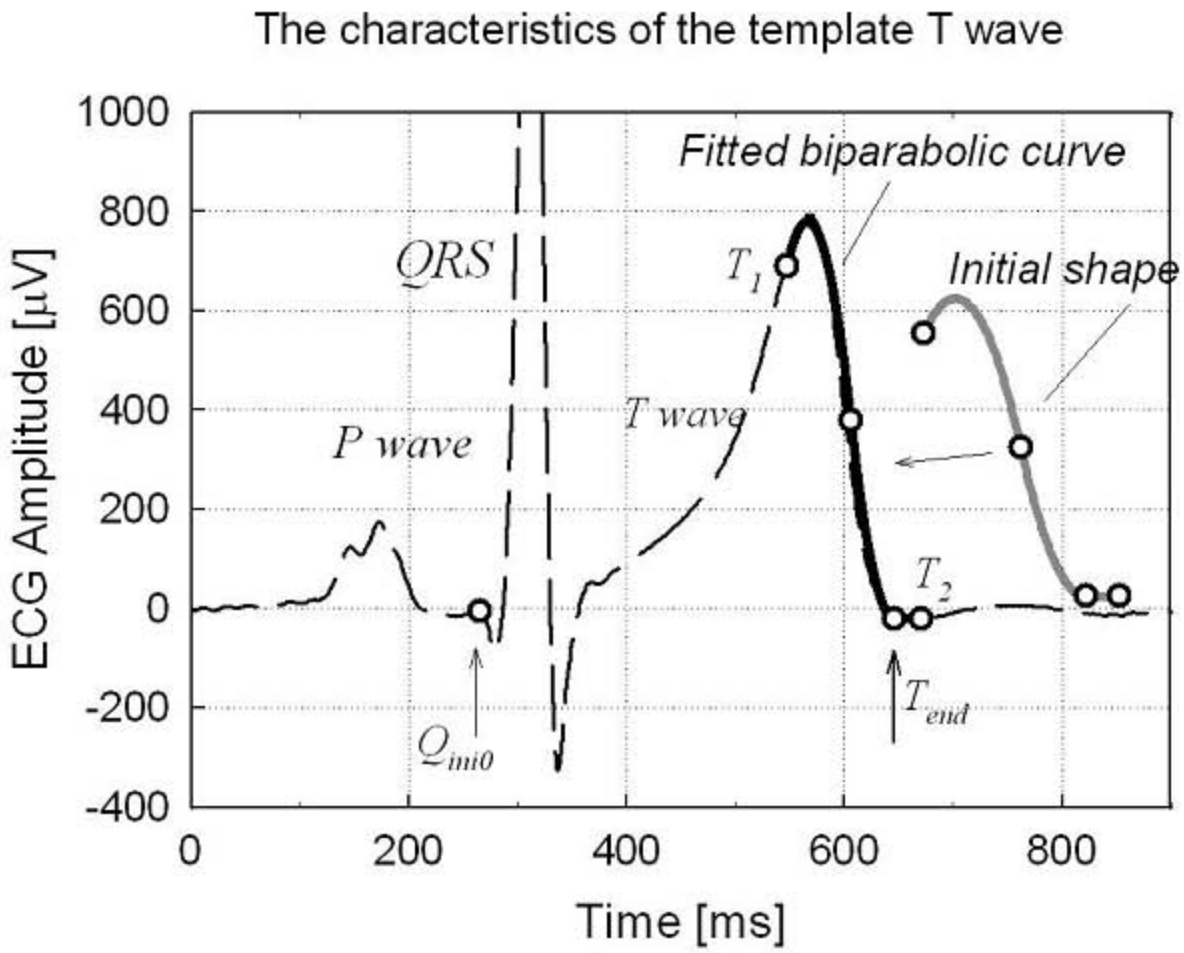
The characteristics of the template T wave
ECG Amplitude [μV]
Time [ms]
1000
800
600
400
200
0
-200
-400
0
200
400
600
800
QRS
P wave
T wave
Fitted biparabolic curve
Initial shape
T_1
T_2
T_{end}
Q_{ini0}

Figure 3a.

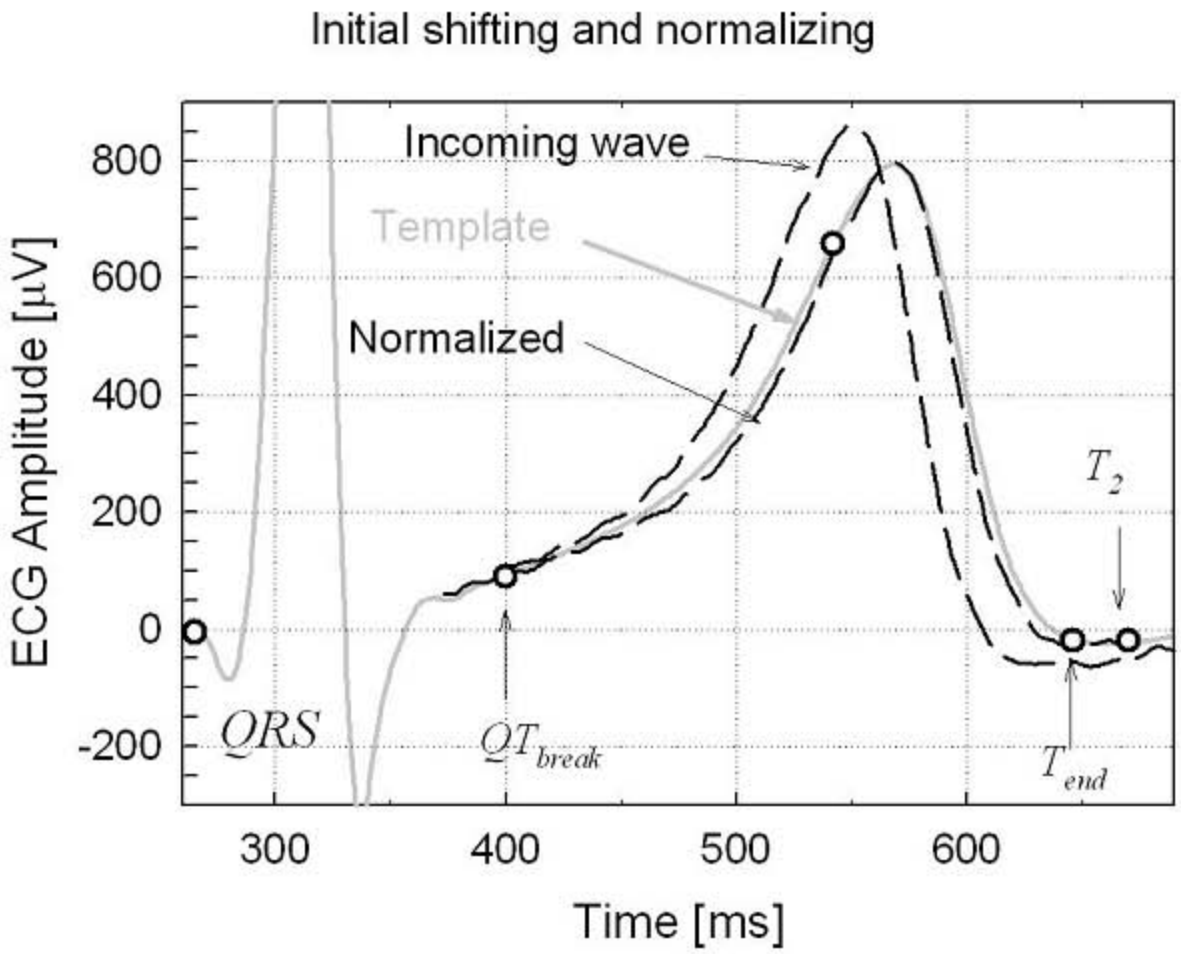
Initial shifting and normalizing
Incoming wave
Template
Normalized
ECG Amplitude [μV]
800
600
400
200
0
-200
QRS
QT_{break}
T_2
T_{end}
300
400
500
600
Time [ms]

Figure 3b.

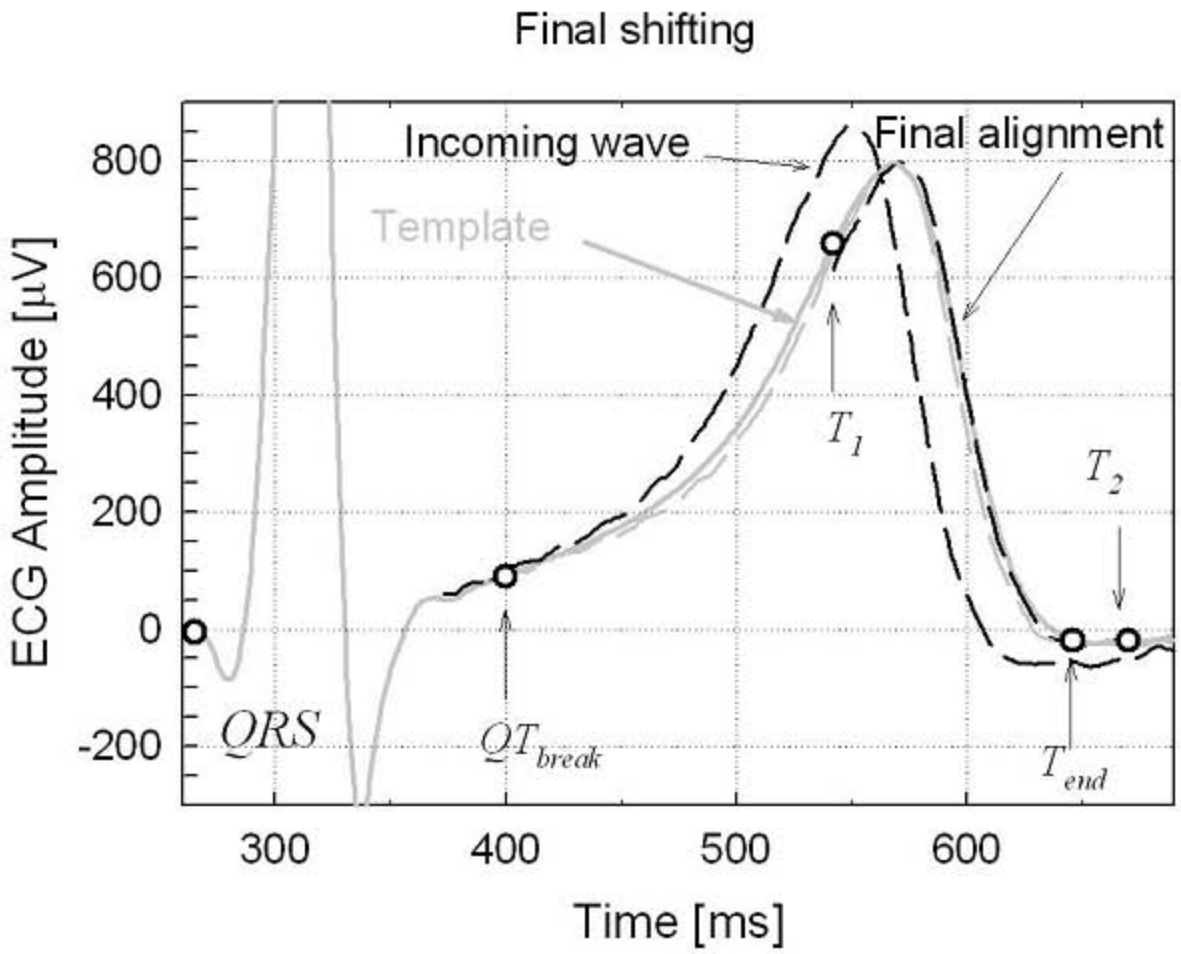
Final shifting
Incoming wave
Final alignment
Template
800
600
400
200
0
-200
ECG Amplitude [μV]
QRS
QT_{break}
T_1
T_2
T_{end}
300
400
500
600
Time [ms]

Figure 4.

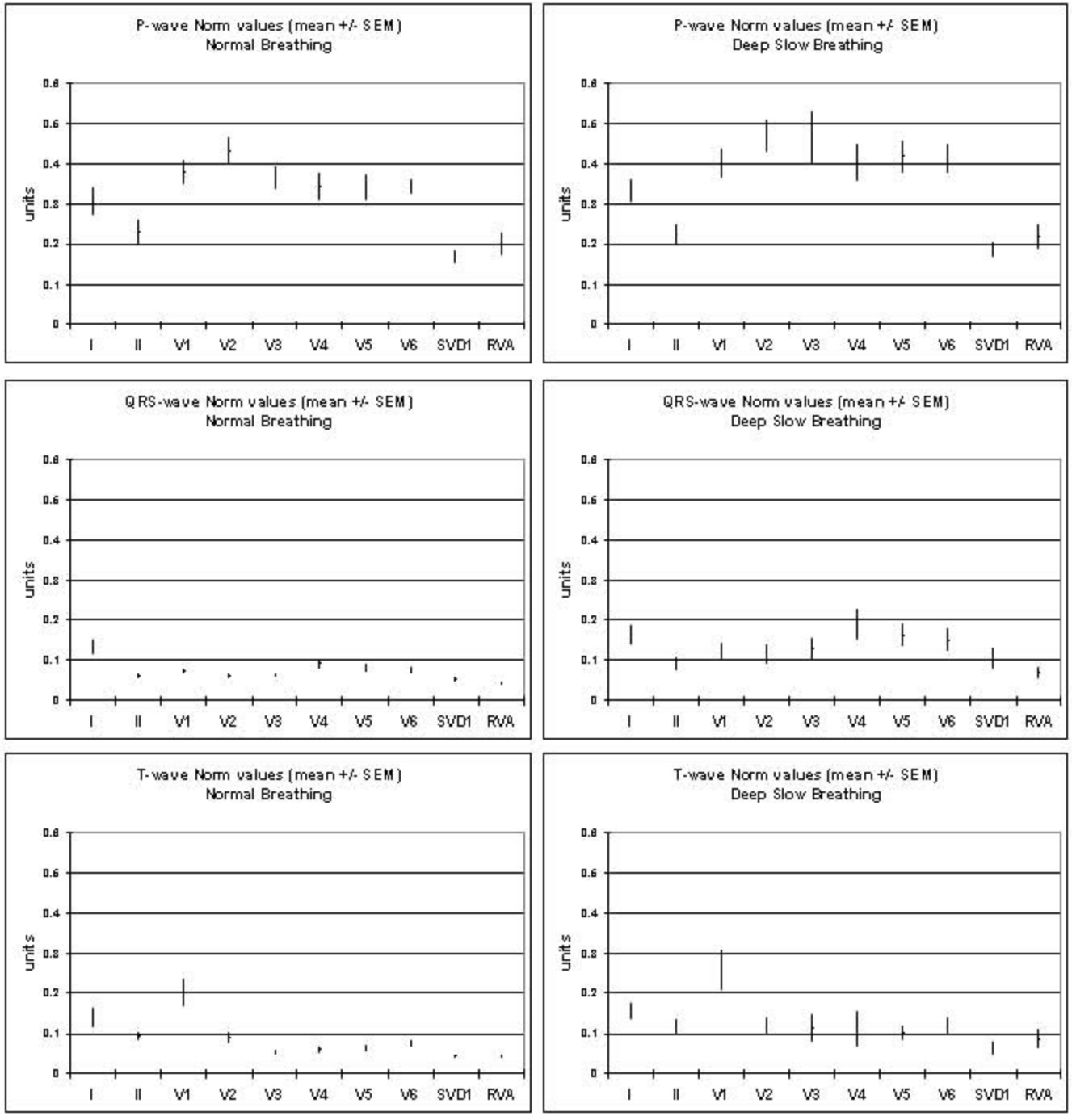
P-wave Norm values (mean +/- SEM)
Normal Breathing
P-wave Norm values (mean +/- SEM)
Deep Slow Breathing
QRS-wave Norm values (mean +/- SEM)
Normal Breathing
QRS-wave Norm values (mean +/- SEM)
Deep Slow Breathing
T-wave Norm values (mean +/- SEM)
Normal Breathing
T-wave Norm values (mean +/- SEM)
Deep Slow Breathing
units
0
0.1
0.2
0.3
0.4
0.6
0.8
I
II
V1
V2
V3
V4
V5
V6
SVD1
RVA

Figure 5.

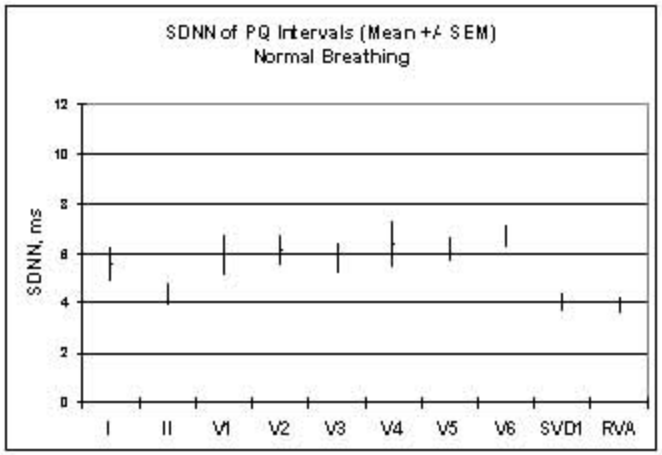
SDNN of PQ Intervals (Mean +/- SEM)
Normal Breathing
SDNN, ms
0
2
4
6
8
10
12
I
II
V1
V2
V3
V4
V5
V6
SVD1
RVA

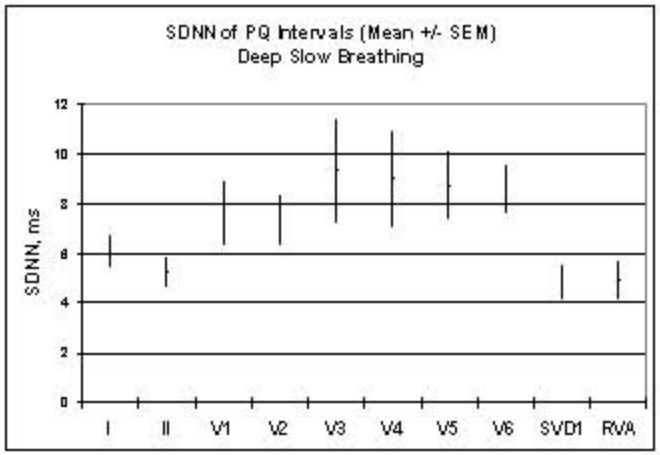
SDNN of PQ Intervals (Mean +/- SEM)
Deep Slow Breathing
SDNN, ms
0
2
4
6
8
10
12
I
II
V1
V2
V3
V4
V5
V6
SVD1
RVA

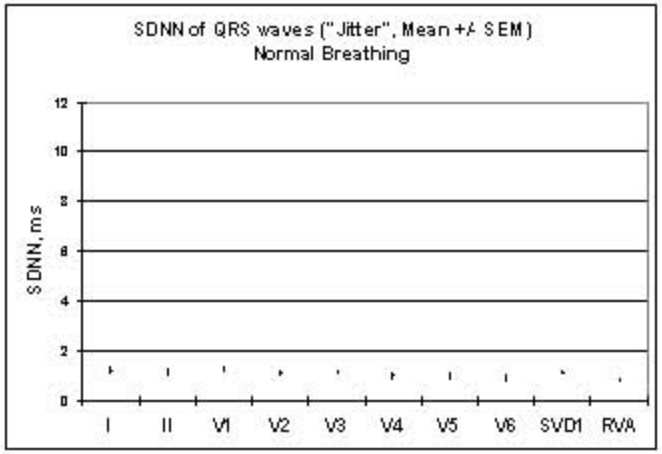
SDNN of QRS waves ("Jitter", Mean +/- SEM)
Normal Breathing
SDNN, ms
0
2
4
6
8
10
12
I
II
V1
V2
V3
V4
V5
V6
SVD1
RVA

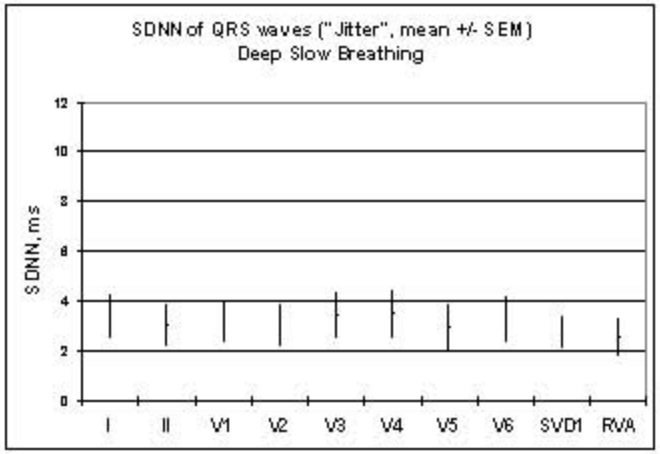
SDNN of QRS waves ("Jitter", mean +/- SEM)
Deep Slow Breathing
SDNN, ms
0
2
4
6
8
10
12
I
II
V1
V2
V3
V4
V5
V6
SVD1
RVA

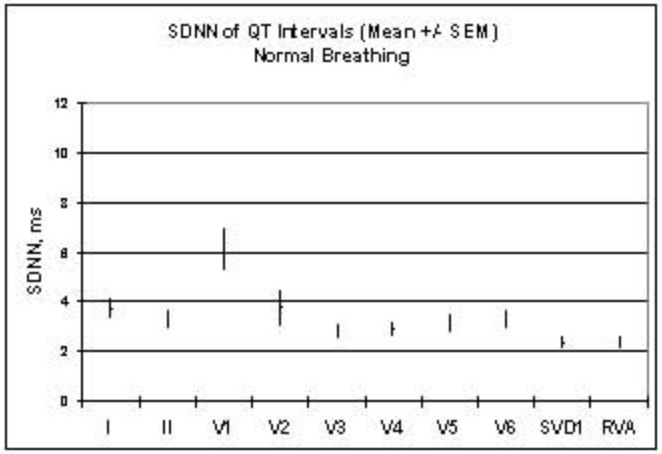
SDNN of QT Intervals (Mean +/- SEM)
Normal Breathing
SDNN, ms
0
2
4
6
8
10
12
I
II
V1
V2
V3
V4
V5
V6
SVD1
RVA

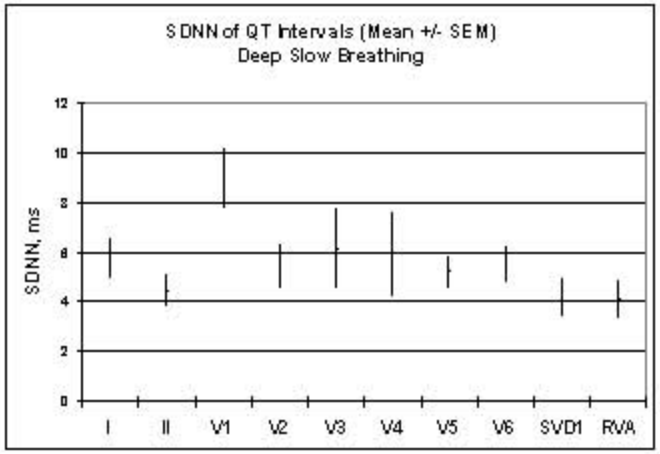
SDNN of QT Intervals (Mean +/- SEM)
Deep Slow Breathing
SDNN, ms
0
2
4
6
8
10
12
I
II
V1
V2
V3
V4
V5
V6
SVD1
RVA

Figure 6.

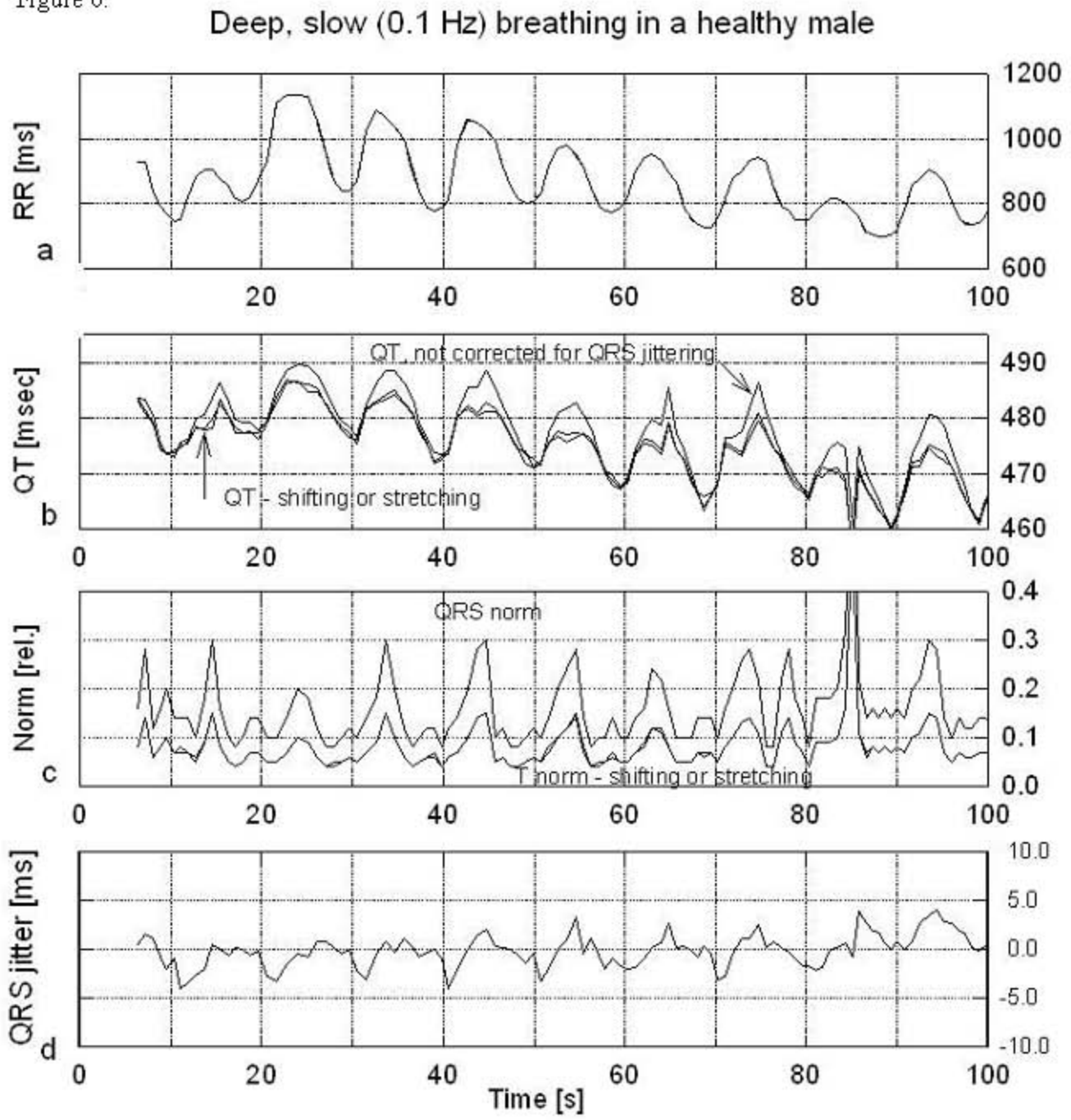
Deep, slow (0.1 Hz) breathing in a healthy male
RR [ms]
a
1200
1000
800
600
20
40
60
80
100
QT [msec]
b
QT, not corrected for QRS jittering
QT - shifting or stretching
490
480
470
460
0
20
40
60
80
100
Norm [rel.]
c
QRS norm
T norm - shifting or stretching
0.4
0.3
0.2
0.1
0.0
0
20
40
60
80
100
QRS jitter [ms]
d
10.0
5.0
0.0
-5.0
-10.0
0
20
40
60
80
100
Time [s]